HHS Public Access

Author manuscript

Toxicology. Author manuscript; available in PMC 2021 October 01.

Published in final edited form as:

Toxicology. 2020 October ; 443: 152561. doi:10.1016/j.tox.2020.152561.

Methylmercury myotoxicity targets formation of the myotendinous junction

Ashley E. Peppriell, **Jakob T. Gunderson**, **Daria Vorojeikina**, **Matthew D. Rand**

Department of Environmental Medicine, University of Rochester School of Medicine and Dentistry, Rochester, NY

Abstract

Methylmercury (MeHg) is a ubiquitous environmental contaminant and developmental toxicant known to cause a variety of persistent motor and cognitive deficits. While previous research has focused predominantly on neurotoxic MeHg effects, emerging evidence points to a myotoxic role whereby MeHg induces defects in muscle development and maintenance. A genome wide association study for developmental sensitivity to MeHg in *Drosophila* has revealed several conserved muscle morphogenesis candidate genes that function in an array of processes from myoblast migration and fusion to myotendinous junction (MTJ) formation and myofibrillogenesis. Here, we investigated candidates for a role in mediating MeHg disruption of muscle development by evaluating morphological and functional phenotypes of the indirect flight muscles (IFMs) in pupal and adult flies following 0, 5, 10, and 15 μM MeHg exposure via feeding at the larval stage. Developmental MeHg exposure induced a dose-dependent increase in muscle detachments (myospheres) within dorsal bundles of the IFMs, which paralleled reductions eclosion and adult flight behaviors. These effects were selectively phenocopied by altered expression of *kon-tiki* (*kon*), a chondroitin sulfate proteoglycan 4/NG2 homologue and a central component of MTJ formation. MeHg elevated *kon* transcript expression at a crucial window of IFM development and transgene overexpression of *kon* could also phenocopy myosphere phenotypes and eclosion and flight deficits. Finally, the myosphere phenotype resulting from 10 μM MeHg was partially rescued in a background of reduced *kon* expression using a targeted RNAi approach. Our findings implicate a component of the MTJ as a MeHg toxicity target which broaden the understanding of how motor deficits can emerge from early life MeHg exposure.

Graphical Abstract

Corresponding Author: Matthew Rand, matthew_rand@urmc.rochester.edu.

CONFLICT OF INTEREST:

The authors have no conflicts of interest to declare.

Declaration of interests

The authors declare that they have no known competing financial interests or personal relationships that could have appeared to influence the work reported in this paper.

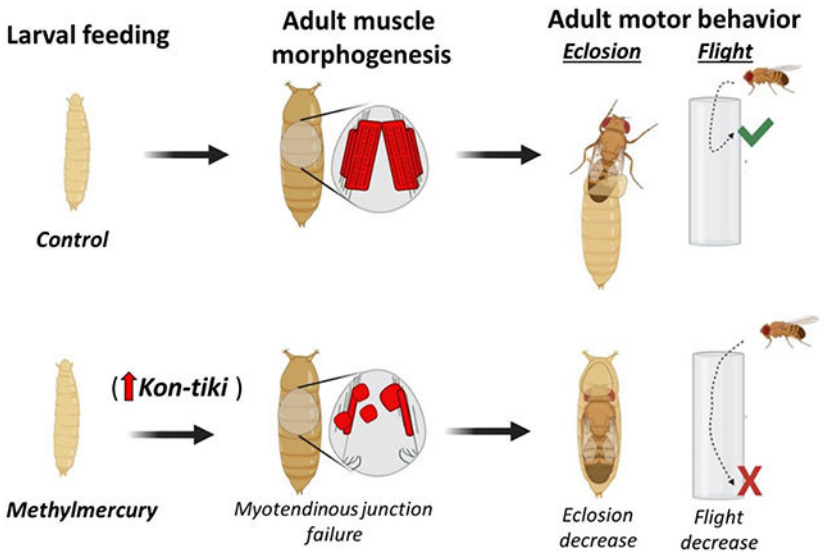

Keywords

Methylmercury; Drosophila; alternative models; myotoxicity; myotendinous junction; developmental toxicity

1. INTRODUCTION

Methylmercury (MeHg) is an especially toxic organic form of mercury (Clarkson 2002) that continues to be a public health concern due to its occurrence in fish and seafood and the unavoidable exposure that comes with human consumption (Committee on Toxicological Effects of Methylmercury 2000). Historic accidental MeHg poisonings have solidified the understanding that the developing fetus is an especially sensitive target and that, at sufficient doses, MeHg can elicit cognitive and motor deficits in children exposed in early life. (Bakir et al. 1973; Matsumoto et al. 1965). While MeHg neurotoxicity has been studied extensively, the discrete developmental targets of MeHg remain to be fully resolved. Among the wide range of neurological deficits that MeHg causes, several involve motor deficits including muscle weakness, abnormal muscle tone and reflexes, rigidity, ataxia, and involuntary movements (Harada 1995; McKeown-Eyssen et al. 1983; Roegge and Schantz 2006). While such motor deficits have primarily been attributed to MeHg neuropathy (Eto et al. 2010; Rodier PM 1984; Sager et al. 1982) (Patel and Reynolds 2013), emerging evidence primarily from our lab supports that MeHg can target skeletal muscle directly, particularly in a developmental context (Engel and Rand 2014; Prince and Rand 2017, 2018; Usuki et al. 1998). For example, proliferating mouse myoblasts fail to differentiate after MeHg exposure, even when the MeHg is removed after a 24-hour exposure (Culbreth and Rand 2020; Prince and Rand 2018). Early studies of prenatally exposed mice showed stark deficits in open field and swimming behavior at one month of age where indices of neurotoxicity including brain weight, protein, choline acetyltransferase and cholinesterase were unaltered (Spyker et al. 1972). Additional studies of MeHg exposures in rats and in zebrafish, revealed myopathology characterized by smaller muscle fiber diameter, increased space between

fibers, and defects in mitochondrial structure and enzyme activity that, in some cases, was distinct from a primary motor neuropathy (de Oliveira Ribeiro et al. 2008; Usuki et al. 1998).

More recent studies employing the Drosophila model have revealed signaling pathways that mediate MeHg perturbation of muscle morphogenesis in development (Engel and Rand 2014) (Montgomery et al. 2014). In a prior study, we conducted a genome wide association study (GWAS) for genes influencing developmental tolerance and susceptibility to MeHg. In this GWAS, phenotyping was based on a dose dependent inhibition of pupal eclosion behavior consequent to MeHg exposure during the larval feeding stage. The GWAS identified clusters of “muscle structure and development” genes. This finding was accompanied by an overt rounded muscle, or “myosphere”, phenotype in the developing adult indirect flight muscles (IFMs) seen in the pupal thorax (Montgomery et al. 2014). We have since demonstrated that MeHg effects on eclosion behavior and IFM myosphere formation can be moderated by targeted transgenes that protect against MeHg toxicity, such as the multi-drug resistance like protein MRP1 and enzymes related to glutathione synthesis and metabolism (Prince et al. 2014; Rand et al. 2019; Vorojeikina et al. 2017). Altogether, these studies have confirmed muscle morphogenesis as a sensitive MeHg target, implicating myogenic contexts which may render an individual particularly susceptible to MeHg toxicity (e.g. genetic polymorphism in a myogenic gene). Nevertheless, the discrete mechanism(s) for this susceptibility remain to be elucidated.

Drosophila IFMs are a well characterized model of muscle development that are strikingly similar in structure and share key developmental processes with vertebrate striated muscles (Fernandes et al. 1991; Schulman et al. 2015; Sink 2006; Spletter et al. 2018). Thus, IFM development has a wider biological significance that can provide insight to parallel mechanisms in vertebrates. The IFMs are required for insect flight function and are comprised of two main muscle groups: the dorsal-longitudinal muscles (DLMs) and dorso-ventral muscles (DVMs). IFM development follows a characteristic timeline of gene expression and morphogenetic events during the pupal life stages, that are best described with the events of DLM formation, as shown in Fig. 1 A - D. Briefly, DLM morphogenesis proceeds sequentially through myoblast fusion, myotube elongation, tendon attachment events, and ultimately myofibrillogenesis at stereotypical time points after pupa formation (h APF). Concurrent with myoblast fusion is the expression of adhesion protein genes *kirre* and *sticks n’ stones (sns*)(Bour et al. 2000; Ruiz-Gomez et al. 2000). Myotube elongation and tendon attachment to form the myotendinous junction (MTJ) (Reedy and Beall 1993) overlap between 24 – 36 h APF and coincide with elevated expression of the CSPG4/NG2 homologue, *kon-tiki (kon)* (Estrada et al. 2007; Schnorrer et al. 2007; Weitkunat et al. 2014). Finally, from approximately 40 h APF onward, MTJ strengthening and myofibrillogenesis are contemporaneous with elevated expression of αPS2-integrin, *inflated (if)* and its heterodimeric partner, βPS-integrin, *myospheroid (mys)* (Fernandes et al. 1996; Perez-Moreno et al. 2017). Remarkably, *kirre, sns, kon,* and *inflated* were all identified in the prior GWAS for MeHg tolerance and susceptibility genes (Montgomery et al. 2014), underscoring the potential for factors involved in muscle development and myotendinous junction formation to be affected by MeHg.

Here, we leverage the Drosophila model to further interrogate several myogenic gene candidates that may confer heightened sensitivity to MeHg, leading to muscle dysmorphology and/or motor deficits. By comparing muscle morphology and behavior defects imparted by developmental exposure to MeHg together with altered expression of candidate genes, we show that MeHg preferentially induces failure in MTJ formation and that *kon* is a potential mediator of methylmercury toxicity during muscle development.

2. METHODS

2.1 Test Substance:

Methylmercury chloride was obtained from Sigma-Aldrich (#215465).

2.2 Drosophila Stocks, culturing and MeHg treatments:

Transgene overexpression and knockdown studies were performed using the Gal4/UAS system (Brand and Perrimon 1993). The following *Drosophila* fly lines were obtained from Bloomington *Drosophila* Stock Center (Indiana University, Bloomington, Indiana): Mef2:RFP (this line is a recombinant of Mef2-Gal4 (#27390) (a “pan-muscle” mesodermal driver); and UAS-RFP-nls) (#38424); mδ:RFP (The *mδ* promoter/enhancer shows restricted expression to the IFM (Prince and Rand 2017), and the line is a recombinant strain of E(Spl)mδ-Gal4 (#47671) and UAS-RFP-nls (#38424)); UAS-kon-RNAi (JF) (#31584) and control w^{1118}(#5905); Canton S. (CS) (#1).The following RNAi lines were obtained from Vienna Drosophila Resource Center (Vienna, Austria): UAS-kon-RNAi (GD) (#37283), UAS-kirre-RNAi (#14476), UAS- if-RNAi (#100770), and UAS-mys-RNAi (#103704, KK line and #29620, GD line). The UAS-HA-kon-FL4-1/TM3 (“kon-HA”), wg-lacZ was a gift of F. Schnorrer (Max Planck Institute of Biochemistry, Martinsried, Germany). These flies contain the full length kon coding sequence with the addition of the wingless (*wg*) signal peptide. Stocks bearing combinations of mutants, reporters, Gal4, or UAS (e.g. Mef2:RFP, *mδ.RFP)* were generated by conventional recombination genetics. All lines were maintained on a standard fly food made of cornmeal, molasses, yeast, and agar, and kept in a humidified chamber at 25°C on a 12/12hr light/dark cycle. In general, MeHg treatments were performed by addition of MeHg to preparations of Jazz Mix fly food (Fisher Scientific, # AS153) prepared in vials as previously described (Rand et al. 2014). MeHg concentrations in the food ranged from 0, 5, 10 and 15 μM, which is equivalent to 0, 1, 2, and 3 ppm MeHg. For reference, tuna and swordfish commonly found at fish counters for human consumption can range from 0.3 - 3 ppm (Groth 2010). Exposures are performed by transferring first-instar larva to vials of MeHg food and developing to the appropriate pupal or adult stage for assays described below.

2.3 Staging of Drosophila pupae:

Pupae were staged as previously described (Bainbridge and Bownes 1981). Timing of developmental events specific to the IFM were obtained from a transcriptomics resource by Spletter et al., 2018, which was also used to validate our to gene-expression patterns (Spletter et al. 2018). We focused our analyses of morphological phenotypes on pupae aged to 49 - 57 h APF, when the growing myofibers have lengthened to span the thorax and are in the midst of undergoing myofibrillogenesis.

2.4 Time-lapse recordings of Drosophila pupae:

White *mδ.RFP* pupae (0 h APF) were removed from the sides of vials and staged to 24 h APF before positioning dorsal side up on a Superfrost microscope slide (VWR International Radnor, PA) and secured ventrally by double-stick tape for live fluorescent reporter imaging. Pupae were enclosed in a handmade humidity chamber to prevent desiccation during the 40-hour time-lapse recording (24 – 64 h APF). Fluorescent images were acquired using a Nikon AZ100 widefield epifluorescent zoom microscope equipped with a X-Y-Z programable stage, 1X objective, and 300 ms exposure settings. Z-dimension focal planes captured at 10 μm steps were assembled with the Extended Depth of Field (EDF) function within the Nikon Elements software. Time-lapse Movies for trios of control and MeHg-treated pupae were each compiled from images captured every 15 minutes.

2.5 Muscle Phenotype Quantifications:

Due to the restricted expression of *E(Spl)mδ* in developing IFM (Prince and Rand 2017), a fly line was generated that co-expresses *E(Spl)mδ-Gal4 and UAS-RFP-nls (mδ.RFP)* and subsequently used to characterize IFM phenotypes under MeHg exposures. *mδ-RFP* larvae were seeded into 0, 5, 10, or 15 μM MeHg food media and monitored until pupae formation. For morphological rescue experiments, *mδ.RFP* was crossed with UAS-kon-*RNAi* or genotype control (*w1118*) and progeny seeded into 0 or 10 μM MeHg food media until white pupae formation (0 h APF). White pupae were removed from the sides of vials and staged to 49 - 57 h APF before removal of the pupal encasing and positioning dorsal side up on a Superfrost microscope slide (VWR International Radnor, PA) for live fluorescent reporter imaging of IFM. Halocarbon-700 oil was added to each pupa to prevent desiccation. Fluorescent images were acquired using a Nikon AZ100 widefield epifluorescent zoom microscope with a 5X objective and consistent exposure settings between each sample. Images were processed using Nikon Elements software and exported as TIF files before being converted to 32-bit images in ImageJ (NIH). Final images were assembled using Microsoft PowerPoint for randomized, blinded scoring of myospheres. The myosphere phenotype was scored if a DLM or DVM presented with a rounded muscle phenotype in the thorax. The data were represented as a continuous variable of total number of myospheres. The *Mef2Gal4>UAS-RFP-nls; UAS-RNAi*-based morphological comparisons were also scored categorically as a proportion of all scored individuals containing one or more myosphere in the IFM region.

2.6 Behavioral Assays: Eclosion

Eclosion is the very first neuromuscular activity of the adult fly, and is defined as emergence of adults from the pupa case. Eclosion rates were determined as previously described (Rand et al. 2014). Briefly, L1 larvae were seeded at 50/vial on food (Jazz Mix, Fisher Scientific, #AS153) containing 0 to 15 μM MeHg, and allowed to develop for 13 days at 25°C. Flies that successfully eclosed were scored and expressed as percent eclosion. Each MeHg exposure condition was assayed in triplicate.

2.7 Dark Pupae Quantifications:

In some cases, eclosion rates were low or completely inhibited by MeHg exposure. As an alternative method to quantify development, the number of individuals that complete metamorphosis to the late pupal stage (scored as 'dark pupa') was used as an additional endpoint to differentiate tolerance to MeHg, as described previously (Rand et al. 2014). Dark pupae (pharate adults) are typically observed when stage 13 (Bainbridge and Bownes 1981) is achieved. The number of individuals reaching dark pupae as scored on day 13 includes adults that successfully eclose as well as pharate adult that are retained in pupa case.

2.8 Behavioral Assays: Flight

Flight tests were performed with minor modifications to those previously described (Babcock, Ganetzky, 2014).The dimensions of the plexi-glass flight column (76.2 cm, 12.7cm diameter, 34 cm circumference and drop column 25.5 cm, 3.2 cm diameter, 10.2 cm circumference were maintained from Babcock and Gnetsky's apparatus, while the funnel and tubes were adjusted for our setup. The diameter of the funnel was 2.3 cm which was flush with the plastic food vials (2.5 cm) used to transmit the flies down the drop column one vial at a time through the funnel and ultimately into the flight cylinder. The flight cylinder was lined with a removable acrylic sheet with paintable adhesive (TangleFoot Tangle-Trap Inc.) to capture flies where they alight after entering the tube. The height at which the fly lands corresponds to the fitness in the flight performance. The adhesive liner is removed to a white surface, imaged, and landing heights of at least 100 flies per group are digitally quantified. Landing heights of individual flies are represented in cm. Flies which fell to the bottom, captured in a mineral oil dish, were categorized as "flightless" and assigned the lowest landing height of 76.2 cm. Before testing, freshly 1 - 2-day old adult males and females were separated on CO_2 and recovered at least 24 h. For MeHg flight tests, adult flies were tested 11 days post-eclosion to allow for residual Hg burden to clear. Flies were kept at 25°C throughout the exposure and recovery periods leading up to testing.

2.9 RNA transcript expression by RT-q-PCR

Changes of the relative expression levels were determined by using the $2^{-\Delta\Delta Ct}$ method (Livak and Schmittgen, 2001) using whole-body RNA extracted from staged pupae in pools of 10. All biological replicates are independent samples of pooled pupae. A 5:1 TRIzol reagent (Invitrogen): chloroform ratio was used to isolate total RNA. The RNA was used to synthesize cDNA using the High-Capacity cDNA Reverse Transcription kit (Fisher #4638813). RT-q-PCR was performed in a Bio-Rad CFX96® Real-Time PCR system using iTaq Universal SYBR® Green Supermix (Bio-Rad, # 1725121). Levels of mRNA were normalized to the ribosomal protein *RP49* housekeeping gene. The following primer sequences were used, represented 5'/3':

RP49: AGTATCTGATGCCCAACATCG / TTCCGACCAGGTTACAAGAAC

Kon-tiki: CCGCCAACA AATCCACTACT / ATGAATTGGAAACGCTTCTTGT

Inflated: GAC ACCTCCCGCTATCAACAG / CTTTGG AGTCGAATGGCA CC

Myospheroid. CAGCAGTCTAAGCTC CTA CTC / GACTGCGGTTGGATTTGGAC

Kirre: TGGACTGGCCATTAATCTTACC / AACGATCGCCACCGAAAT

Mef2: ATATCACGCATCACCGATGAA / GGCGTACTGGTACAGCTTGT

E(Spl)mδ: CCGTTCAGGGTCAGAGATTTAT / CCTTGAGTTCGTCCAGATACAG

2.10 Statistical Analyses:

Statistical analyses were done in JMP. Comparisons of treatment and/or genotype were evaluated in relation to untreated control strains or respective genetically manipulated crosses, or Gal4 > UAS crosses to their relevant control strain or cross, as indicated. For eclosion assays, a two-tailed Z-test was conducted for each concentration categorically, as the percent of flies successfully eclosed is a non-continuous value reaching 0% and 100% at the minima and maxima, respectively. Landing heights from the flight assay were evaluated using between groups ANOVA's to compare the effects of MeHg treatment, genotype, and/or sex, where appropriate. Morphological analyses that quantified the number of myospheres as a proportion of all observed pupae were analyzed using a Chi-Square analysis. Morphological analyses that quantified the total number of myospheres in the thorax of 49 - 57 h APF pupae were analyzed using between groups ANOVAs with comparisons between treatment and/or genotype, where appropriate. When variables did not meet parametric assumptions (i.e. not normally distributed or presented with heteroscedasticity), a non-parametric Mann–Whitney–Wilcoxon or Kruskal-Wallis or test was applied. Values are represented as an average of at least three replicates ± standard error. In all cases, $p \leq 0.05$ were considered to be significant.

3. RESULTS

Since IFM development in the pupal thorax proceeds through a well-characterized sequence of events (Fernandes et al. 1991; Schulman et al. 2015; Sink 2006; Spletter et al. 2018, Fig. 1 A - D), we sought to identify which of these events might be most sensitive to MeHg. We implemented time-lapse microscopy of IFM development in control and MeHg exposed pupae using *mδ:RFP* as a fluorescent reporter to reveal IFM morphology over a dynamic period of muscle development from 24 – 64 hours after pupa formation (h APF) (Fig. 1 A - B, Videos S1,S2). The time-lapse recording of control pupae revealed a growing intensity of the red fluorescent protein (RFP) signal between 24 and 36 hr APF (Fig. 1 E), consistent with an anticipated profile of fusion of *mδ.RFP* expressing myoblasts with the larval scaffold muscles. This initial period is also marked with a transient longitudinal compaction of the nascent myofibers (Fig. 1 E arrows mark boundaries of myofibers). Subsequently, a robust elongation of the DLM myofibers between 36 and 48 hr was seen, an event that is enabled by stable attachments to tendon cell filipodia. (Fig. 1 E). At 64 hr APF the DLM fibers were seen to extend successfully to the anterior and posterior regions of the thorax, indicating stable tendon anchorage (Fig. 1 E, arrows). With MeHg exposure (10 μM) the developing DLMs underwent a similar enhanced expression of RFP and longitudinal compaction over the 24 - 36 hr period as was seen in control pupae (Fig. 1 F). In several instances, the subsequent myofiber extension event following compaction was interrupted

with an apparent retraction of the fiber, which consequentially condensed into a rounded muscle, or myosphere. Frequently, the myosphere was seen to localize near the anterior or posterior attachment site (Fig. 1 F). In some instances, myospheres are seen to move freely among the residual fibers that maintain attachment (Fig. 1 F, white chevrons, Video S2). This myosphere phenotype was also evident in the DVM muscles (Fig. 1 F, Video S2). In some instances, DVM were not detected, possibly indicating the resulting myosphere has receded ventrally from the dorsal attachment site, hence leaving the imaging field. In the IFM of pupae exposed to 10 μM MeHg, the first myospheres were observed at approximately 36 h APF (Fig. 1 F), which coincides with the process of myotube compaction (Fig. 1 C). Myosphere numbers appeared to peak at approximately 48 h APF (Fig. 1 F), thus, we subsequently used this time point to determine a MeHg dose dependent relationship for this phenotype. Between 0 - 15 μM MeHg, we observed a dose-dependent increase in number of myospheres (Fig.2 A - E).

To further asses how this muscle phenotype might influence motor function we examined eclosion behavior and flight behavior. In *mδ.RFP* flies used for quantifying myospheres, we saw a parallel dose-dependent reduction in eclosion rate, resulting in virtually no eclosion (less than 1%) at the 15 μM MeHg treatment level (Fig.2 F). Despite the reduction in eclosion, there was no significant change in the percent of dark pupae formed by day 13 of pupation (Fig.2 G), indicating that individuals on 10 – 15 μM MeHg developed to late stage pupae, but ultimately failed to emerge from the pupa case. This observation suggested that the underlying development of adult structures required for eclosion (i.e muscles) are perturbed by MeHg.

We further assessed motor function with flight behavior, for the reasons that 1) the requirement of the IFMs in eclosion behavior is uncertain (Delinger 1994; Miyan 1989) and 2) we wanted to evaluate if effects could be elicited at lower (2 - 5 μM MeHg) doses. Flight assays were performed with wild-type *Canton S (CS)* flies, which exhibit a ≥ 85% eclosion rate on 5 μM MeHg (Mahapatra et al. 2010), thereby permitting sufficient number of flies to test flight function at this dose and below. Whereas untreated *CS* flies primarily landed in the top 16 cm of the flight column, developmental exposure to MeHg led to a significant drop in landing height from the top of the column in both males and females (Fig.2 H - I). For males, landing height was significantly reduced from an average of 11.6 ± 7.5 cm in untreated controls to an average of 22.2 ± 19.0 cm and 36.0 ± 23.5 cm for adults raised on 2 and 5 μM MeHg, respectively (Fig.2 H). In females, flight was significantly reduced at the 5 μM MeHg dose, as landing height from the top dropped from an average of 17.5 ± 9.6 cm in untreated controls to an average of 51.5 ± 23.9 cm on 5 μM MeHg (Fig.2 I).

To identify the potential cause of the MeHg myospheres, we reasoned that phenotypes accessed from systemic knockdown of key genes that function across the developmental timeline of IFM morphogenesis would yield a phenotype that most resembles that induced by MeHg. We therefore investigated the effects of knockdown of *kirre, kon, inflated,* and *myospheroid.* Using the Mef2Gal4 driver, considered “pan-muscle”, in combination with a UAS-RFP-nls reporter (*Mef2:RFP*), the morphological effect of RNAi knockdown of *kirre, kon, or inflated* was visualized in the IFM of 48 - 57 h APF pupae. Myosphere number and frequency were scored as the occurrence of rounded muscles visible in the IFM and the

proportion of pupae that demonstrated one or more myospheres in the IFMs, respectively. For comparison, pupae scored following larval exposure to 10 μM MeHg yielded an average of 8 – 9 myospheres in the IFM for > 90% of individuals (Fig 3B, F), compared to 5% in untreated controls (Fig. 3A, F). Pan-muscle knockdown of *kirre* resulted in few myospheres with comparable number and frequency to untreated controls (Fig 3A, C, F). Interestingly, pan-muscle knockdown of *kon* phenocopied MeHg treatment with a comparable number of myospheres (approximately eight) and frequency of 85% (Fig. 3B, D, F). With *if* knockdown, myospheres were observed in 26.7% of pupae (Fig. 3E, F). The knockdown of *Mys* proved lethal at the embryonic and wandering larval stages, thus the pupal phenotype was unable to be scored.

To investigate whether consequences of compromised Kon function extend to neuromuscular behavior, eclosion and flight behaviors were evaluated after *kon* knockdown. Using the Mef2Gal4 driver to express two independent RNAi hairpins against *kon,* eclosion rate was reduced to 45% using the *kon-RNAi* GD construct, and to 36% using the JF construct (Fig. 4A). These effects paralleled the apparent reduction in whole animal *kon* transcript levels assessed by RT-qPCR (Fig. 4C). The JF construct was more efficient and was therefore used for subsequent analyses. To focus our analyses of *kon* to the IFM, the mδGal4 driver was used to express the *kon-RNAi* (JF construct) in an IFM-restricted manner. Eclosion rate was not affected by IFM-restricted knockdown of *kon* (Fig. 4 B, D). Nevertheless, this result enabled sufficient numbers of adult flies with which to test flight function. The flight performance of both male and female adult *mδGal4>kon-RNAi* flies was significantly reduced in comparison to genotype controls (Fig. 4 E, F, Table S2), where average male and female landing height were shifted by approximately 10 cm compared to genotype controls (*mδGal4>w1118)* and about 11% were completely flightless in both sexes (Table S2). Additionally, the morphology of the IFM following restricted knockdown of *kon* was visualized using mδGal4 driver that co-expresses *UAS-RFP-nls (mδ.RFP).* The resulting IFM morphology of *mδ:RFP>UAS-kon-RNAi* pupae was indistinguishable from that of genotype controls (Fig. 4 G, H). Altogether, these data indicate that compromised *kon* expression, which is known to induce a failure in MTJs, adversely effects IFM morphology and neuromuscular functions of eclosion and flight similar to the effect of MeHg.

We next explored the possibility that MeHg might act on *kon* more directly to produce the myosphere and neuromuscular behavioral phenotypes. To test for this, we analyzed *kon* transcript expression levels in response to MeHg exposure by RT-qPCR using whole animal RNA collected at several pupal timepoints. *Kon* expression was also compared to expression of *kirre, if, mys,* to assess specificity in *kon* response. The concentration of 10 μM was selected because it is the lowest concentration tested that induces the myosphere phenotype in over 90% of pupae (Fig.2 C,E, Fig.3 B). Timepoints along the developmental trajectory of the IFM were chosen to capture key windows of muscle morphogenesis.

In untreated controls, *kirre, kon,* and *if* showed an anticipated profile of sequential peaks in expression: *kirre* at 20 - 24 h APF, *kon* at 24 - 48 h APF and *if* at > 48 h APF. MeHg treatment did not significantly alter gene expression of *kirre* at any timepoint relative to the untreated control (Fig.5 A). However, a significant increase in *kon* expression was evident at the 24 h APF timepoint (Fig.5 B). *Inflated* trended toward a two-fold reduction in gene

expression at 72 h APF (Fig.5 C). Whereas *mys* demonstrated a relatively consistent gene expression level across pupal development, no significant change was observed with MeHg treatment (Fig.5 D).We examined two additional key myogenic genes, *E(spl)mδ* and *Mef2.* We have previously shown that the *Notch* target gene, *E(spl)mδ* is upregulated at early pupal timepoints following exposure to 10 μM MeHg (Prince and Rand 2017); it was included in our analysis as a positive control. Consistent with our previous report, we observed a significant elevation of *E(spl)mδ* at 20 h APF window following MeHg exposure (Fig.5 E). *Mef2* is a master regulator of myogenic gene expression that is known to control several genes (including *kirre* and *if)* that contribute to IFM development (Caine et al. 2014; Sandmann et al. 2006). *Mef2* was therefore included in our analysis to ascertain if MeHg effects were targeting events genetically upstream of the GWAS candidates. No significant MeHg-induced changes were observed at any timepoint for *Mef2* (Fig.5 F). In summary, the data support that *kon* expression is moderately enhanced by MeHg during a specific interval of pupal development.

To determine if the MeHg-induced elevation in *kon* (Fig.5 B) is related to the morphological and functional phenotypes that result from MeHg, we evaluated if *kon* overexpression would impair eclosion and flight functions, as well as perturb muscle morphology. To examine this, we overexpressed kon using the Mef2Gal4 and mδGal4 drivers that differ in their strength and distribution in the muscle domain, as well as temporal expression profiles. The Mef2Gal4>UAS-kon-HA combination was able to significantly impair eclosion rate to about 20% (Fig. 6A) following an almost 3-fold increase in *kon* gene expression indicated by RT-PCR analysis (Fig. 6B). Using the Mef2:RFP driver to visualize the muscle morphology, overexpression of *kon* showed a robust appearance of myospheres in comparison to genotype controls (Fig. 6C, D). Although myospheres were observed in approximately 80% of *Mef2:RFP>UAS-kon-HA* pupae examined (*data not shown)*, aberrant muscle lengthening and structural perturbation was apparent in all individuals, pointing to a high penetrance that is not lethal until the pupa stage. In contrast to our observations with the pan-muscle manipulations, restricting *kon* overexpression to the IFM using mδ-Gal4 did not reduce eclosion rate (Fig. 6E) despite successful upregulation of *kon* in whole-pupal RNA extracts (Fig. 6F).

Moreover, visualizing IFM morphology using the mδ-Gal4 driver in combination with an RFP reporter (*mδ.RFP*), was indistinguishable from genotype control pupae (Fig. 6G, H). Interestingly, we found drastic impairments in flight performance after IFM-restricted *kon* overexpression, which was significantly reduced in both males and females (Fig. 6 I, J). Additionally, for both male and female flies, the average landing height were shifted by over 40 cm, and over 55% of individuals were entirely flightless (Table S3).

The above findings suggest that the myosphere phenotype is particularly sensitive to a narrow range of *kon* expression. Thus, if outcomes of MeHg exposure are mediated through elevated *kon* expression, we reasoned that an initial reduction in *kon,* within the range where no IFM myospheres are induced (Fig.4 H), should in turn rescue the subsequent effects of MeHg. To test this, we expressed *UAS-kon-RNAi* with the mδ-Gal4 driver in combination with a UAS-RFP-nls reporter to achieve a restricted and milder knockdown of *kon.* We then assessed the effects of 10 μM MeHg exposure on the resulting number of IFM myospheres.

The reduced level of *kon* expression significantly reduced the number of myospheres subsequently induced by 10 μM MeHg (Fig.7 A - E).

4. DISCUSSION:

In this study, we expand upon prior evidence that developing muscle is sensitive to MeHg toxicity and implicate the myotendinous junction (MTJ) as a discrete target. Using time-lapse microscopy images of IFM development, we resolve that MeHg exposure in developing Drosophila can subsequently induce myospheres in adult flight muscles that are first visible at approximately 36 h APF in both the DLMs and DVMs and peak in number between 48 – 55 h APF. The dose-dependent increase in DLM myospheres observed in 48 – 55 h APF coincided with a dose-dependent reduction in eclosion rate, suggesting that the phenotype in the flight muscles reflects a more general perturbation of muscle morphogenesis that could extend to other muscle groups, such as those required for eclosion. At lower doses of larval MeHg treatments, below that which induce IFM myospheres, significant reduction in adult flight performance was observed in both males and females.

The IFM myospheres we observe are most consistent with a failure of myotube-tendon targeting and attachment. In support of this, we found that, among a select pool of candidate myo-morphogenesis genes identified in a prior GWAS, *kon* overexpression and knockdown was able to recapitulate functional and morphological phenotypes of MeHg developmental exposure. Independent of MeHg exposure, these results imply a sensitive homeostatic mechanism whereby excessive or insufficient *kon* is able to impair MTJ development. To our knowledge, this is the first study demonstrating failure of the adult MTJ with *kon* overexpression. Of note, overexpression of *kon* in Drosophila embryos reportedly results in excessive filopodial projections and consequential mis-attachments of larval myotubes (Ferreira 2016). This may implicate a mechanism by which MeHg exerts its effects through *kon.* Furthermore, we determined that MeHg specifically elevated *kon* expression at a critical developmental window (24 h APF). The trajectory of gene expression for other genes assessed (*kirre, if, mys, mef2)* was not significantly altered by MeHg, suggesting against global increase in gene expression as a consequence of MeHg, and emphasizing the specificity of *kon* as a potential MeHg target. Finally, we observed that the MeHg-induced myosphere phenotype is partially rescued by IFM-restricted reduction in *kon* expression, supporting the hypothesis that MeHg acts through Kon to mediate the formation of myospheres in the developing flight muscle.

These findings suggest MeHg may engage Kon to alter MTJ formation and yield myospheres in the IFM. Kon is an orphan single-pass transmembrane neurexin family member that is expressed in developing muscle of *Drosophila (Estrada et al. 2007; Schnorrer et al. 2007).* Its vertebrate homologue is a chondroitin sulfate proteoglycan 4(CSPG4)/NG2 protein, that is best known for its expression in oligodendrocyte progenitor cells, but is transiently expressed in early post-natal muscle and is upregulated in certain forms of muscular dystrophy (Petrini et al. 2003; Petrini et al. 2005). In *Drosophila, kon* is required for MTJ formation during development of many muscles, including the IFM (Weitkunat et al. 2014). Kon is essential for muscle attachment to tendon cells, and is required for integrin accumulation a the MTJ, which contributes added strength of attachment (Lemke and

Schnorrer 2017; Schulman et al. 2015). Indeed, *kon* is most highly expressed during the attachment initiation and attachment maturation phases (Contrino et al. 2012; Spletter et al. 2018), this work). Interestingly, we observed that the first instances of myospheres following larval MeHg treatment coincide with timepoints of maximal *kon* expression and functional requirement in the IFM (Fig.1 F). There is a substantial increase in the amount of tension across the MTJ in the DLM at this time (Weitkunat et al. 2014), as the myotubes have attached to tendons and must maintain their anchorage when the myotube undergoes compaction to approximately a third of its length (Lemke and Schnorrer 2017). Thus, if the nascent MTJ is unable to withstand the force of tension, it would detach from tendon and recoil to form a myosphere. Consistent with our data, others have reported that genetic knockdown of *kon* is able to induce a recoiled myosphere phenotype in DLM (Weitkunat et al. 2014) and in other muscle groups (Estrada et al. 2007; Perez-Moreno et al. 2014; Perez-Moreno et al. 2017; Schnorrer et al. 2007). Thus, one possibility is that MeHg acts on Kon itself to disrupt extracellular adhesion protein interactions at the muscle-tendon interface. As the binding partner for Kon remains uncertain, this will require additional characterization of Kon interactions. Alternatively, MeHg may perturb intracellular scaffolding proteins that interact with Kon to localize it and induce downstream signaling cascades for muscle development. For example, in *Drosophila,* Kon couples to the PDZ-protein dGRIP to mediate MTJ attachment (Estrada et al. 2007; Schnorrer et al. 2007) and loss-of function mutations in *dGRIP* and *kon* both result a myosphere phenotype (Swan et al. 2004). In preliminary experiments, we observe that RNAi knockdown of *dGRIP* results in IFM myospheres (data not shown). The possible role of dGRIP in mediating MeHg effects remains an interesting future line of inquiry. It is of note that at lower MeHg doses, where IFM myosphere phenotypes are not readily apparent, adult flies, nonetheless, display deficits in flight performance. We attribute this to a developmental defect, as the residual MeHg in the adults is not sufficient to perturb flight function (*data not shown*). One possibility is that although MTJs are of sufficient strength to form and anchor the flight muscles, upon incurring the demands of flight the MTJs fail, and render the flight muscles ineffective. Future studies aimed at characterizing adult IFM morphology will shed light on this by identifying events of MTJ formation that are particularly sensitive to MeHg. Alternatively, MeHg could directly target one of several cellular processes required for muscle integrity; notably, adhesion protein turnover and maintenance. Adhesion proteins have been implicated as targets for metal and MeHg toxicity (Prozialeck et al. 2002), and mis-regulation of integrin turnover has been shown to disrupt MTJ attachment in *Drosophila* (Pines et al. 2012). Discerning the structural versus physiological effects of MeHg at these lower dose exposures will be an important future investigation, especially as it may more accurately reflect chronic low dose MeHg exposure that is more apt to occur with humans. Nevertheless, identifying genes involved in heightened susceptibility to MeHg (e.g. *kon)* can translate to interindividual responses to MeHg exposure influenced by genetic differences in vertebrate homologues (e.g. *NG2*).

One limitation of this study is that the myosphere phenotype we observe could potentially be mediated by failing tendon cells, which we have yet to explore. Nonetheless, Kon expression is reported to be restricted to the tips of myotubes, and not in tendon cells (Maartens and Brown 2015), supporting the notion of a muscle-specific effect. We have also not addressed

a potential role for the accompanying motor neurons known to innervate the IFMs in this study. Fernandes *et al.* showed that the intersegmental nerve (ISN) maintains contact with the larval scaffold muscles of the growing DLM, serving as a guide for migrating myoblasts and facilitating their eventual fusion with the growing DLM (Fernandes and Keshishian 1998). In the early timepoints of our time lapse analysis, we observe a robust accumulation of RFp signal at the site of the forming DLM, which we attribute to the bulk fusion of RFP-expressing myoblast to the larval scaffold muscles of the DLM (Fig. 1 F), indicating ISN mediated myoblast migration and subsequent fusion events are intact. The role of the ISN in maintaining the progression of MTJ formation and myofibrillogenesis remains to be elaborated, particularly in the context of MeHg toxic exposure.

In summary, this study is the first to implicate a component of the MTJ as a MeHg toxicity target. Our results broaden the understanding of how motor deficits can emerge in the case of an early life MeHg exposure by illustrating how targets within muscle morphogenesis can complement the conventional understanding of neural susceptibility with respect to MeHg toxicity. We anticipate these findings will inform the process of identifying the corollary targets, and windows of susceptibility, in mammalian neuromuscular development.

Supplementary Material

Refer to Web version on PubMed Central for supplementary material.

ACKNOWLEDGEMENTS:

We thank the University of Rochester researchers for communal fly husbandry supplies and critical feedback on the project during meetings, including I. Krout, and D. Bergstralh. We also thank D. Cory-Slechta for statistics advice and E. Smolock for feedback on the manuscript. We appreciate the Drosophila community as a whole for maintaining curated databases, and are especially grateful to F. Schnorrer for providing us with *kon* fly strains.

FUNDING:

This study was supported by National Institute of Environmental Health Sciences [R01 ES025721 (PI; M.D.R.), P30 ES001247 (co-I; M.D.R.)] and the University of Rochester Environmental Health Center [T32207026 (A.E.P)].

References

1. Bainbridge SP and Bownes M 1981 Staging the metamorphosis of Drosophila melanogaster. J Embryol Exp Morphol 66, 57–80. [PubMed: 6802923]
2. Bakir F, Damluji SF, Amin-Zaki L, Murtadha M, Khalidi A, al-Rawi NY, Tikriti S, Dahahir HI, Clarkson TW, Smith JC and Doherty RA 1973 Methylmercury poisoning in Iraq. Science 181,230–241. [PubMed: 4719063]
3. Bour BA, Chakravarti M, West JM and Abmayr SM 2000 Drosophila SNS, a member of the immunoglobulin superfamily that is essential for myoblast fusion. Genes Dev 14, 1498–1511. [PubMed: 10859168]
4. Brand AH and Perrimon N 1993 Targeted gene expression as a means of altering cell fates and generating dominant phenotypes. Development. 118, 401–415. [PubMed: 8223268]
5. Caine C, Kasherov P, Silber J and Lalouette A 2014 Mef2 interacts with the Notch pathway during adult muscle development in Drosophila melanogaster. PLoS One 9, e108149. [PubMed: 25247309]
6. Clarkson TW 2002 The three modern faces of mercury. Environ Health Perspect 110 Suppl 1, 11–23. [PubMed: 11834460]
7. Committee on Toxicological Effects of Methylmercury, N.R.C.o.t.U.S. 2000 Toxicological effects of methylmercury, National Academies Press, Washington.

8. Contrino S, Smith RN, Butano D, Carr A, Hu F, Lyne R, Rutherford K, Kalderimis A, Sullivan J, Carbon S, Kephart ET, Lloyd P, Stinson EO, Washington NL, Perry MD, Ruzanov P, Zha Z, Lewis SE, Stein LD and Micklem G 2012 modMine: flexible access to modENCODE data. Nucleic Acids Res 40, D1082–1088. [PubMed: 22080565]

9. Culbteth M and Rand MD 2020 Methylmercury modifies temporally expressed myogenic regulatory factors to inhibit myoblast differentiation. Toxicol In Vitro 63, 104717. [PubMed: 31706035]

10. de Oliveira Ribeiro CA, Nathalie MD, Gonzalez P, Yannick D, Jean-Paul B, Boudou A and Massabuau JC 2008 Effects of dietary methylmercury on zebrafish skeletal muscle fibres. Environ Toxicol Pharmacol 25, 304–309. [PubMed: 21783867]

11. Delinger DL 1994 Metamorphosis behavior in flies. Annu Rev Entomol 39, 243–266. [PubMed: 8135500]

12. Engel GL and Rand MD 2014 The Notch target E(spl)mdelta is a muscle-specific gene involved in methylmercury toxicity in motor neuron development. Neurotoxicol Teratol 43, 11–18. [PubMed: 24632433]

13. Estrada B, Gisselbrecht SS and Michelson AM 2007 The transmembrane protein Perdido interacts with Grip and integrins to mediate myotube projection and attachment in the Drosophila embryo. Development 134, 4469–448. [PubMed: 18039972]

14. Eto K, Marumoto M and Takeya M 2010 The pathology of methylmercury poisoning (Minamata disease): The 50th Anniversary of Japanese Society of Neuropathology. Neuropathology 30, 471–479. [PubMed: 20500453]

15. Fernandes J, Bate M and Vijayraghavan K 1991 Development of the indirect flight muscles of Drosophila. Development 113, 67–77. [PubMed: 1765009]

16. Fernandes JJ, Celniker SE and VijayRaghavan K 1996 Development of the indirect flight muscle attachment sites in Drosophila: role of the PS integrins and the stripe gene. Dev Biol 176, 166–184. [PubMed: 8660859]

17. Fernandes JJ and Keshishian H 1998 Nerve-muscle interactions during flight muscle development in Drosophila. Development 125, 1769–1779. [PubMed: 9521914]

18. Ferreira I.R.d.S. 2016 Molecular role of Kon-tiki during myotube migration and attachment. Ludwig Maximilian University of Munich, Max-Planck-Institut für Biochemie, Martinsried (München).

19. Groth E 3rd. 2010 Ranking the contributions of commercial fish and shellfish varieties to mercury exposure in the United States: implications for risk communication. Environ Res 110, 226–236. [PubMed: 20116785]

20. Harada M 1995 Minamata disease: methylmercury poisoning in Japan caused by environmental pollution. Crit Rev Toxicol 25, 1–24. [PubMed: 7734058]

21. Lemke SB and Schnorrer F 2017 Mechanical forces during muscle development. Mech Dev 144, 92–101. [PubMed: 27913119]

22. Maartens AP and Brown NH 2015 The many faces of cell adhesion during Drosophila muscle development. Dev Biol 401,62–74. [PubMed: 25596335]

23. Mahapatra CT, Bond J, Rand DM and Rand MD 2010 Identification of methylmercury tolerance gene candidates in Drosophila. Toxicol Sci 116, 225–238. [PubMed: 20375079]

24. Matsumoto H, Koya G and Takeuchi T 1965 Fetal Minamata disease. A neuropathological study of two cases of intrauterine intoxication by a methyl mercury compound. J Neuropathol Exp Neurol 24.

25. McKeown-Eyssen GE, Ruedy J and Neims A 1983 Methyl mercury exposure in northern Quebec. II. Neurologic findings in children. Am J Epidemiol 118, 470–479. [PubMed: 6637974]

26. Miyan JA 1989 The thoracic mechanism for eclosion and digging during the extrication behaviour in Diptera Phyiological Entomology 14, 309–317.

27. Montgomery SL, Vorojeikina D, Huang W, Mackay TF, Anholt RR and Rand MD 2014 Genome-wide association analysis of tolerance to methylmercury toxicity in Drosophila implicates myogenic and neuromuscular developmental pathways. PLoS One 9, e110375. [PubMed: 25360876]

28. Patel E and Reynolds M 2013 Methylmercury impairs motor function in early development and induces oxidative stress in cerebellar granule cells. Toxicol Lett 222, 265–272. [PubMed: 23948120]
29. Perez-Moreno JJ, Bischoff M, Martin-Bermudo MD and Estrada B 2014 The conserved transmembrane proteoglycan Perdido/Kon-tiki is essential for myofibrillogenesis and sarcomeric structure in Drosophila. J Cell Sci 127, 3162–3173. [PubMed: 24794494]
30. Perez-Moreno JJ, Espina-Zambrano AG, Garcia-Calderon CB and Estrada B 2017 Kon-tiki enhances PS2 integrin adhesion and localizes its ligand, Thrombospondin, in the myotendinous junction. J Cell Sci 130, 950–962. [PubMed: 28104814]
31. Petrini S, Tessa A, Carrozzo R, Verardo M, Pierini R, Rizza T and Bertini E 2003 Human melanoma/NG2 chondroitin sulfate proteoglycan is expressed in the sarcolemma of postnatal human skeletal myofibers. Abnormal expression in merosin-negative and Duchenne muscular dystrophies. Mol Cell Neurosci 23, 219–231 [PubMed: 12812755]
32. Petrini S, Tessa A, Stallcup WB, Sabatelli P, Pescatori M, Giusti B, Carrozzo R, Verardo M, Bergamin N, Columbaro M, Bernardini C, Merlini L, Pepe G, Bonaldo P and Bertini E 2005 Altered expression of the MCSP/NG2 chondroitin sulfate proteoglycan in collagen VI deficiency. Mol Cell Neurosci 30, 408–417. [PubMed: 16169245]
33. Pines M, Das R, Ellis SJ, Morin A, Czerniecki S, Yuan L, Klose M, Coombs D and Tanentzapf G 2012 Mechanical force regulates integrin turnover in Drosophila in vivo. Nat Cell Biol 14, 935–943. [PubMed: 22885771]
34. Prince L, Korbas M, Davidson P, Broberg K and Rand MD 2014 Target organ specific activity of drosophila MRP (ABCC1) moderates developmental toxicity of methylmercury. Toxicol Sci 140, 425–435. [PubMed: 24863968]
35. Prince LM and Rand MD 2017 Notch Target Gene E(spl)mdelta Is a Mediator of Methylmercury-Induced Myotoxicity in Drosophila. Front Genet 8, 233. [PubMed: 29379520]
36. Prince LM and Rand MD 2018 Methylmercury exposure causes a persistent inhibition of myogenin expression and C2C12 myoblast differentiation. Toxicology 393, 113–122. [PubMed: 29104120]
37. Prozialeck WC, Grunwald GB, Dey PM, Reuhl KR and Parrish 2002 Cadherins and NCAM as potential targets in metal toxicity. Toxicol Appl Pharmacol 182, 255–265. [PubMed: 12183105]
38. Rand MD, Montgomery SL, Prince L and Vorojeikina D 2014 Developmental toxicity assays using the Drosophila model. Curr Protoc Toxicol 59, 1 12 11–20.
39. Rand MD, Vorojeikina D, Peppriell A, Gunderson J and Prince LM 2019 Drosophotoxicology: Elucidating Kinetic and Dynamic Pathways of Methylmercury Toxicity in a Drosophila Model. Frontiers in Genetics 10.
40. Reedy MC and Beall C 1993 Ultrastructure of developing flight muscle in Drosophila. II. Formation of the myotendon junction. Dev Biol 160, 466–479. [PubMed: 8253278]
41. Rodier PM, A. M, Sager PR. 1984 Mitotic Arrest in the Developing CNS After Prenatal Exposure to Methylmercury. Neurobehavioral toxicology and teratology 6, 379–385. [PubMed: 6514102]
42. Roegge CS and Schantz SL 2006 Motor function following developmental exposure to PCBS and/or MEHG. Neurotoxicol Teratol 28, 260–277. [PubMed: 16487679]
43. Ruiz-Gomez M, Coutts N, Price A, Taylor MV and Bate M 2000 Drosophila dumbfounded: a myoblast attractant essential for fusion. Cell 102, 189–198. [PubMed: 10943839]
44. Sager PR, Doherty RA and Rodier PM 1982 Effects of methylmercury on developing mouse cerebellar cortex. Exp Neurol 77, 197–193.
45. Sandmann T, Jensen LJ, Jakobsen JS, Karzynski MM, Eichenlaub MP, Bork P and Furlong EE 2006 A temporal map of transcription factor activity: mef2 directly regulates target genes at all stages of muscle development. Dev Cell 10, 797–807. [PubMed: 16740481]
46. Schnorrer F, Kalchhauser 1 and Dickson BJ 2007 The transmembrane protein Kon-tiki couples to Dgrip to mediate myotube targeting in Drosophila. Dev Cell 12, 751–766. [PubMed: 17488626]
47. Schulman VK, Dobi KC and Baylies MK 2015 Morphogenesis of the somatic musculature in Drosophila melanogaster. Wiley Interdiscip Rev Dev Biol 4, 313–334. [PubMed: 25758712]
48. Sink H 2006 Muscle Development in Drosophila, Landes Bioscience, Georgetown, TX.

49. Spletter ML, Barz C, Yeroslaviz A, Zhang X, Lemke SB, Bonnard A, Brunner E, Cardone G, Basler K, Habermann BH and Schnorrer F 2018 A transcriptomics resource reveals a transcriptional transition during ordered sarcomere morphogenesis in flight muscle. Elife 7.
50. Spyker JM, Sparber SB and Goldberg AM 1972 Subtle consequences of methylmercury exposure: behavioral deviations in offspring of treated mothers. Science 177, 621–623. [PubMed: 5049306]
51. Swan LE, Wichmann C, Prange U, Schmid A, Schmidt M, Schwarz T, Ponimaskin E, Madeo F, Vorbruggen G and Sigrist SJ 2004 A glutamate receptorinteracting protein homolog organizes muscle guidance in Drosophila. Genes Dev 18, 223–237. [PubMed: 14729572]
52. Usuki F, Yasutake A, Matsumoto M, Umehara F and Higuchi I, 1998 The effect of methylmercury on skeletal muscle in the rat: a histopathological study. Toxicol Lett 94, 227–232. [PubMed: 9609326]
53. Vorojeikina D, Broberg K, Love TM, Davidson PW, van Wijngaarden E and Rand MD 2017 Editor's Highlight: Glutathione S-Transferase Activity Moderates Methylmercury Toxicity During Development in Drosophila. Toxicol Sci 157, 211–221. [PubMed: 28184905]
54. Weitkunat M, Kaya-Copur A, Grill SW and Schnorrer F 2014 Tension and force-resistant attachment are essential for myofibrillogenesis in Drosophila flight muscle. Curr Biol 24, 705–716. [PubMed: 24631244]

Highlights

- Methylmercury (MeHg) perturbs muscle development in *Drosophila melanogaster.*
- Developmental exposure to MeHg impairs eclosion and flight behaviors.
- MeHg perturbs flight muscle morphology by disrupting the myotendinous junction.
- Gene expression of the NG2/CSPG4 homologue, *kon-tiki,* is elevated by MeHg.
- Targeted overexpression of *kon-tiki* in muscle phenocopies MeHg effects.

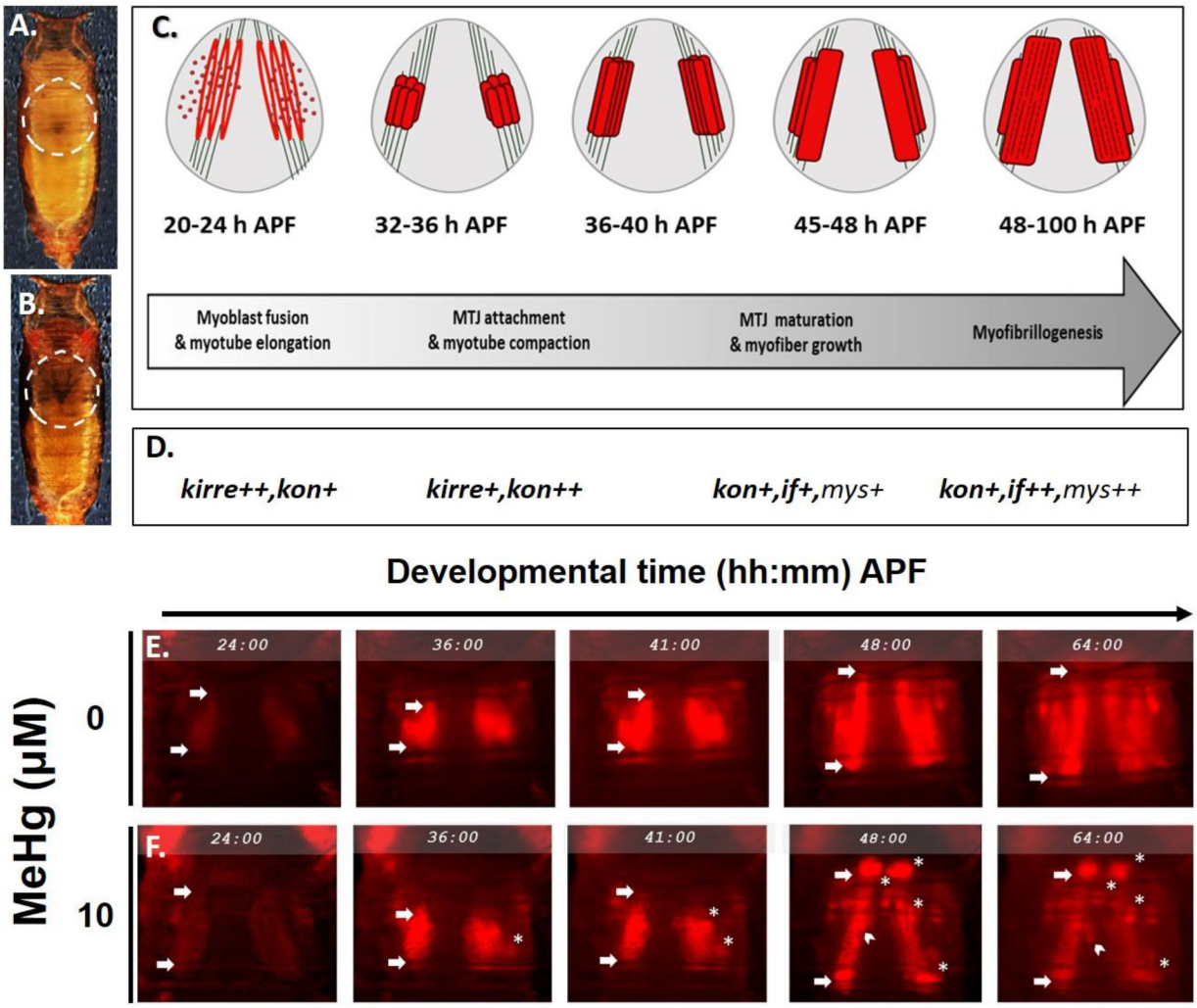

Fig. 1. Model overview: Indirect flight muscle (IFM) development and methylmercury perturbations.

(A - B) Dorsal view of *Drosophila* pupae under white light at (A) 24 hours after pupa formation (h APF) and (B) 64 h APF to show the dark pupa stage preceding eclosion. Dashed circles indicate the thorax. (C – D) Cartoon timeline of major myo-morphogenic events of the dorsal longitudinal flight muscles (DLM). Approximate levels of gene expression at each window are indicated by +'s and GWAS candidates in bold font. Heterotypic, directional myoblastfusion requires *kirre* and occurs from 8 - 24 h APF. The myofibers reach full length at 24 h APF to initiate myotube-tendon attachment and form the myotendinous junction (MTJ) before myotube compaction occurs from 32 - 36 h APF. Myotube elongation and attachment initiation require *kon.* Attachment maturation continues through 48 h APF as additional adhesion proteins (e.g. integrins *inflated(if)* and *myospheroid (mys))* assemble at the MTJ, at which point myofibrillogenesis proceeds. (E – F) Time-lapse still images from *mδ.RFP* pupae over the course of IFM development at 24, 36, 41, 48, and 64 hours h APF in (E) control (F) or 10 μM MeHg-treated conditions. Arrows of each panel indicate anterior and posterior attachments of the dorsal myotube. White asterisks (*) demarcate myospheres, while the white chevrons show a change in

position in free-moving myospheres. Annotations are limited the left hemithorax. This figure can be viewed in color online. (Additional time lapse movies of (E) and (F) can be viewed in supplementary material online)

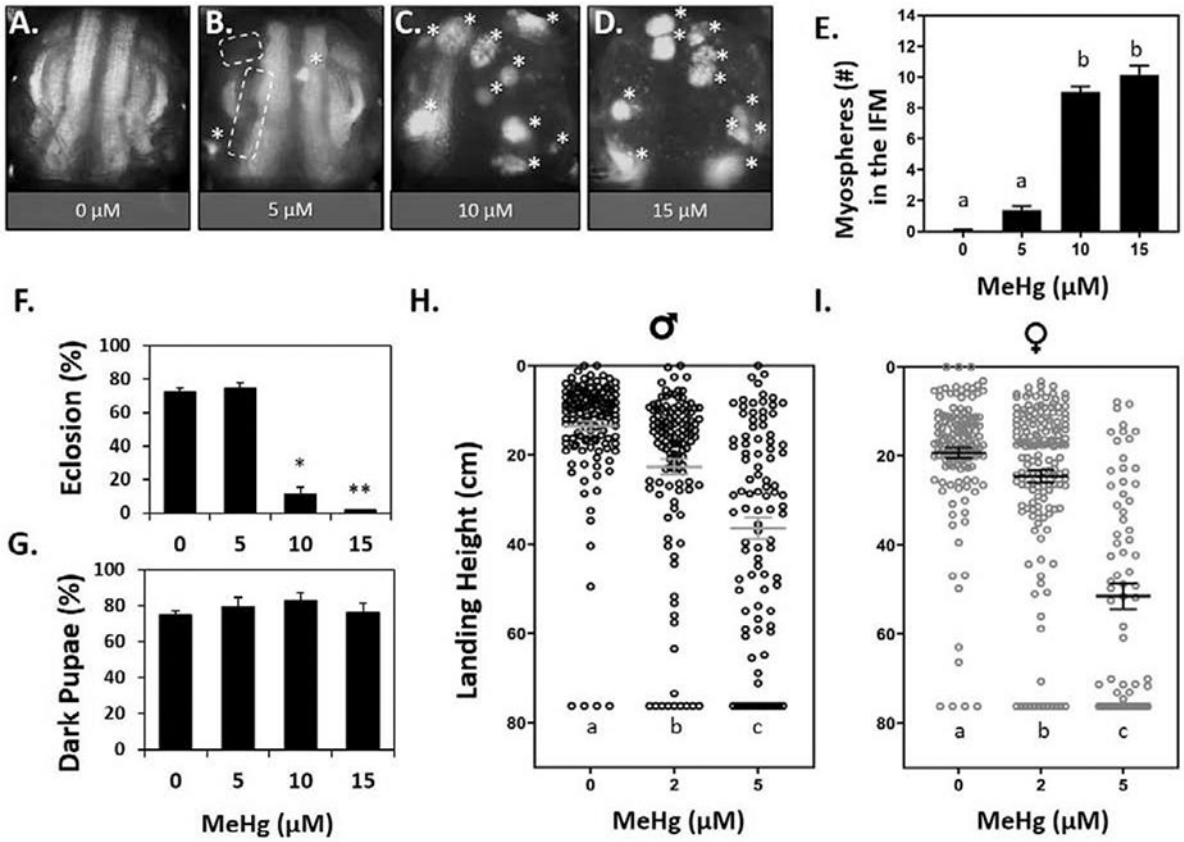

Fig. 2. Dose responsive IFM morphological and flight function defects following larval exposure to MeHg.

(A - D) Representative images of 49 - 57 h APF *mδ:RFP* pupae treated with 0, 5, 10, or 15 µM MeHg. Asterisks (*) indicate average number of myospheres per treatment. Dashed lines indicate missing DVM group. (E) Quantification of myospheres in the IFM ($n \geq 23$ pupae per treatment, letters indicate pair-wise significant differences where $p < 0.05$, ANOVA). (F) Eclosion function (represented as a percent) in *mδ:RFP* flies decreases with increasing MeHg exposure, and G) the percent of these individuals that developed to dark pupae by day 13 ($n = 150$ pupae per treatment, *$p < 0.05$, **$p < 0.001$, Z-test). (H - I) Landing height of male (H) and female (I) wildtype *(Canton S.)* adults after larval exposure to 0, 2, or 5 µM MeHg. Horizontal bars represent mean landing height ± SEM for each group ($n \geq 100$ flies per treatment, letters indicate pair-wise significant differences where $p < 0.05$, Kruskal-Wallace, Dunn's post-hoc for multiple comparisons).

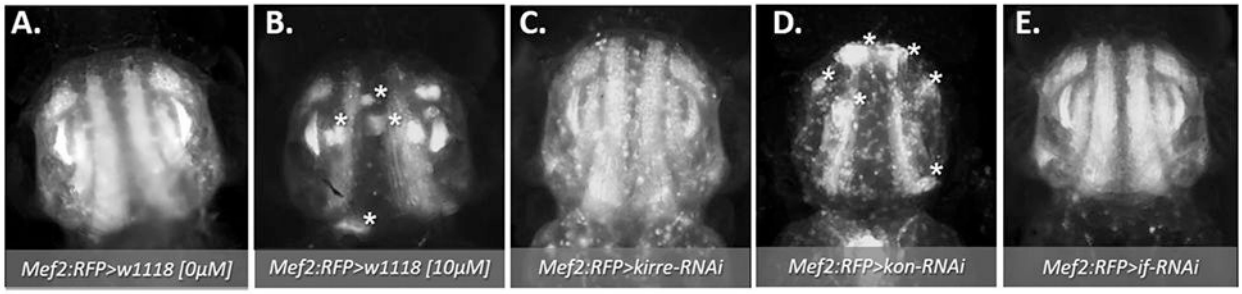

F.

Genotype, [MeHg]	Frequency of IFM myosphere (%)	No. IFM Myospheres (mean + SD)	ANOVA*
Mef2Gal4>UAS-RFP;w1118, [0 μM]	5.00	0.12 0.54	a
Mef2Gal4>UAS-RFP;w1118, [10 μM]	90.91	8.19 3.90	b
Mef2Gal4>UAS-RFP;UAS-kirre-RNAi [0 μM]	7.50	1.95 3.27	a
Mef2Gal4>UAS-RFP;UAS-kon-RNAi [0 μM]	89.29	7.74 4.06	b
Mef2Gal4>UAS-RFP;UAS-if-RNAi [0 μM]	26.67	3.00 3.09	c

*Kruskal-Wallis test, Dunn's post-hoc

Fig. 3. Morphological effects on IFMs following larval MeHg exposure or muscle-restricted knockdown of myotendinous junction (MTJ) gene candidates.

(A - F) Representative epifluorescence images of 49 - 57 h APF pupal thoraces ($n \geq 20$ images per genotype), where asterisks (*) indicate myospheres. (A, B) *Mef2:RFP>w1118* (genotype control) with or without prior larval exposure to 10 μM MeHg; (C - E) *Mef2:RFP>UAS-RNAi* lines against key myogenic genes: (C) myoblast fusion gene, *kirre-RNAi*, or the MTJ genes, (D) *kon-RNAi,* or (E) *if-RNAi.* The number of asterisks in each image correspond to the average number of myospheres observed for each genotype. (F) Quantification of the frequency and average number ± SD of myospheres observed in the IFM for each genotype and treatment. Frequency of myospheres are represented as a percentage of the indicated number of pupae scored per group. Letters indicate pairwise significant differences in average number of myospheres between each group, where $p < 0.05$, $n = 20 – 39$, Kruskal-Wallis test with Dunn's post-hoc for multiple comparisons.

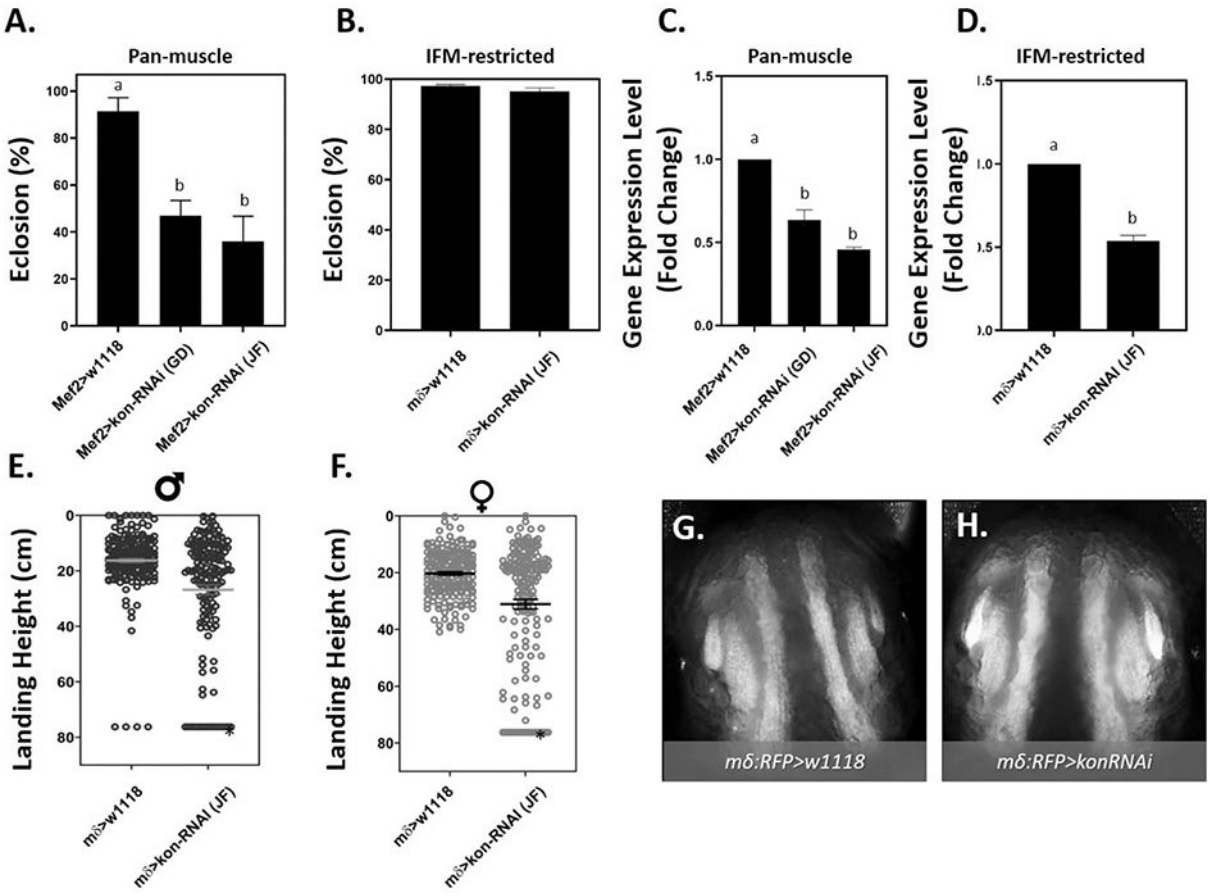

Fig 4. Eclosion and flight defects following RNAi-mediated knockdown of *kon-tiki (kon)*.

(A - B) Average percent eclosion ± SEM following (A) pan-muscle or (B) IFM-restricted knockdown of *kon* compared to genotype controls. Letters indicate pair-wise significant differences where $p < 0.01$, ANOVA, n = 150 pupae per treatment. (C - D) RT-PCR quantification of knockdowns showing average ± SEM of log-2-fold changes in gene expression. Letters indicate pair-wise significant differences, where $p < 0.05$, ANOVA, n = 3 pooled samples). (E - F) Flight function following IFM-restricted knockdown of *kon* in (E) adult male and (F) female *mδ>kon-RNAi(JF)* or *mδ>w1118* flies. The horizontal line and error bars represent mean ± SEM of each sex. Asterisks indicate pair-wise significant differences where $p < 0.01$ (Mann-Whitney test, $n \geq 100$ flies per group). (G – H) Representative images of IFM morphology from 49 - 57 h APF pupae following (H) IFM-restricted knockdown of *kon* (*mδ:RFP>kon-RNAi)* compared to (G) control (*mδ:RFP>w1118*).

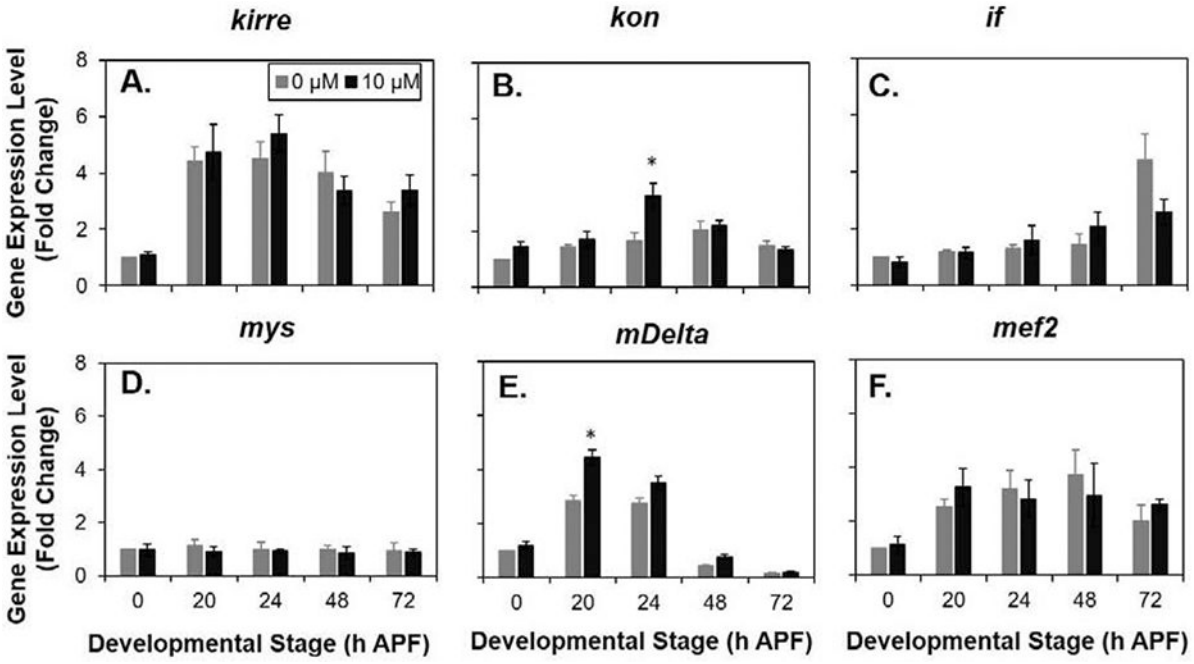

Fig. 5. Effect of MeHg on Expression of Myogenic Genes at Key Stages of MTJ Development.

Gene transcript levels with and without 10 μM MeHg of (A) *kirre,* (B) *kon* (C) *if* (αPS2-integrin), (D) *mys* (*βPS integrin*), (E) *E(Spl6),* and (F) *Mef2* analyzed by RT-PCR at the indicated timepoints. Each data point is normalized to untreated at the first timepoint (0 h APF). ($n \geq 4$; Two-way ANOVA with Sidak's test for multiple comparisons $^*p < 0.05$ in comparison to 0 μM exposure).

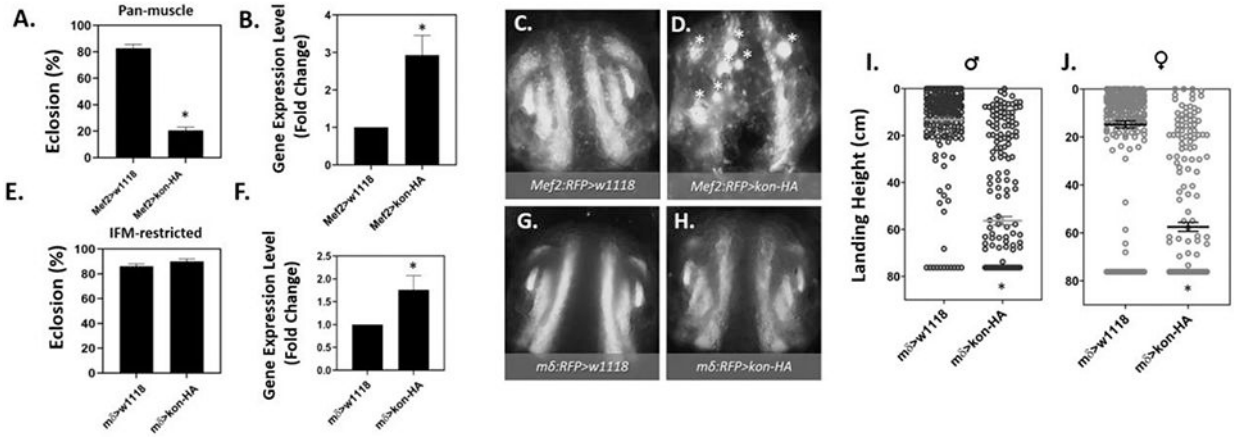

Fig. 6. Eclosion and flight defects following overexpression of kon.

(A - D) Panmuscle *kon* overexpression. A) Eclosion ability is reduced by 72% in *Mef2>Kon-HA* compared to *Mef2>w1118* controls (*p < 0.01, Z-test, n = 150 pupae per group. B) RT-q-PCR quantification of average ± SEM log-2-fold change in *kon* expression *Mef2>Kon-HA* pupae compared to *Mef2>w1118* controls, significant difference indicated by asterisk (*) where p < 0.05, t-test, n = 3 independent samples. (C) The morphology of control *Mef2:RFP>w1118* pupal IFM compared to D) *Mef2:RFP>kon-HA* at 49 – 57 h APF. White asterisks (*) indicate myospheres. (E - J) IFM-restricted overexpression of kon. E) Eclosion ability does not differ between control (*mδ>w1118*) and (*mδ>kon-HA*). F) RT-q-PCR quantification of the average ± SEM log-2-fold change in gene expression of *kon* in *mδ>kon-HA* pupae compared to *mδ>w1118* controls, significant difference indicated by asterisk (*) where p < 0.05, T-test, n = 3 independent samples. G) The morphology of the pupal IFM with in control pupae and H) *kon* overexpression (*mδ:RFP>kon-HA)* is indistinguishable. I) Flight function in adult males and J) females is significantly reduced. Each point is the landing height of an individual fly, and the mean ± SEM is indicated by the horizontal black line and error bars. Asterisks indicate pair-wise significant differences where p < 0.01 (Mann-Whitney test, n ≥ 100 flies per group).

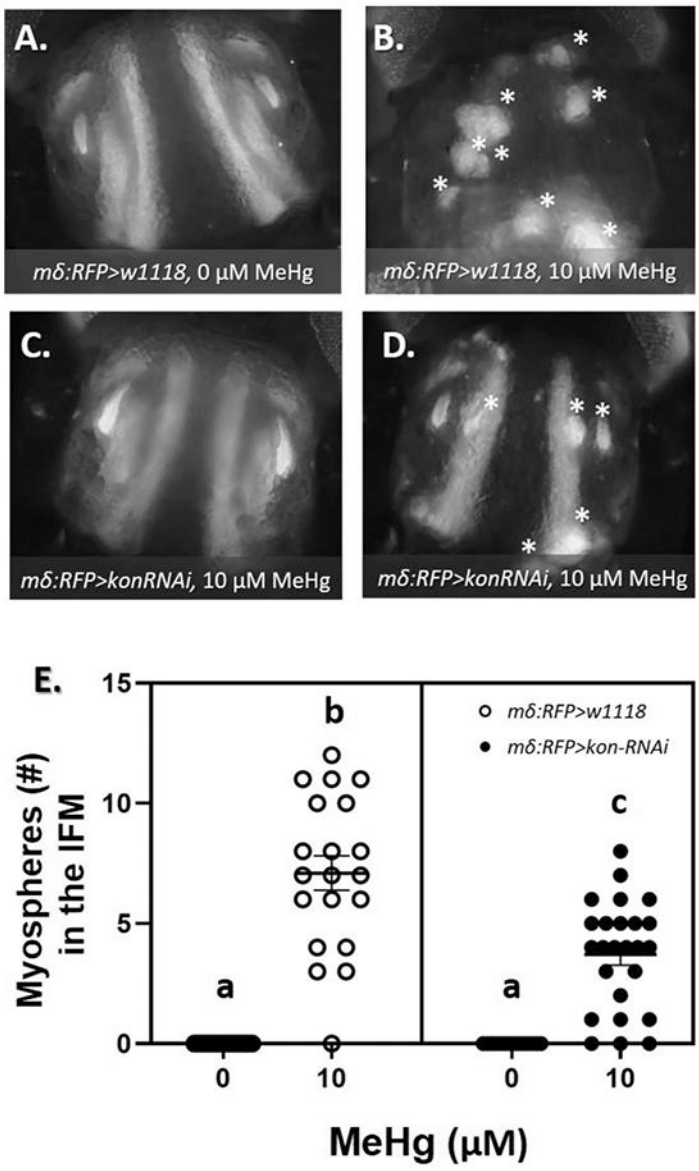

Fig. 7. Frequency of IFM morphological phenotypes after combined MeHg exposure and reduced levels of *kon*.

(A - D) Representative images of 49 - 57 h APF pupae after IFM-restricted *kon* knockdown (*mδRFP>w1118* or *mδRFP>kon-RNAi*) and 0 or 10 μM larval MeHg exposure. At least 20 images were taken per group. Asterisks (*) indicate myospheres in the IFM. (E) Quantification of the average ± SD number of myospheres in the IFM reveal a partial rescue of the muscle attachment phenotype induced by developmental exposure to 10 μM MeHg. Letters indicate pair-wise significant differences where $p < 0.001$ (Two-way ANOVA with Tukey's HSD, $n > 20$ pupae per group).